Acta Cryst. (1988). A44, 864-870

Electron Microscope Analyses of Domains and Discommensurations in Ferroelectric Rb_2ZnCl_4

BY K. TSUDA, N. YAMAMOTO* AND K. YAGI

Physics Department, Tokyo Institute of Technology, Oh-okayama, Tokyo 152, *Japan*

(*Received* 7 *December* 1987; *accepted* 25 *April* 1988)

Abstract

Image contrast of domains and discommensurations in ferroelectric Rb_2ZnCl_4 is studied. Six domains of the two orientation variants and three translation variants in the ferroelectric phase are observed. However, only two kinds of domain boundaries, which are the discommensurations in the incommensurate phase of Rb_2ZnCl_4, are observed. These observations agree with group-theoretical considerations of the phase transition from the normal phase to the commensurate phase of Rb_2ZnCl_4.

1. Introduction

McMillan (1975) first proposed the concept of discommensuration (DC) in incommensurate (IC) phases of crystals and stressed its important role in the phase transition between IC and commensurate (C) phases. Later, DC's were directly observed by Fung, McKernan, Steeds & Wilson (1981) and Chen, Gibson & Fleming (1982) for the case of $TaSe_2$-2*H* using low-temperature electron microscope techniques. There, the DC's and 'dislocations' of the DC lattice (the DC lattice is one-dimensional in the stripe phase of $TaSe_2$-2*H*) were studied. Since then, DC's and 'dislocations' have been reported for various dielectrics such as $NbTe_4$ (Mahy, Van Landuyt, Amelinckx, Uchida, Bronsema & Van Smaalen, 1985), quartz (Dolino, Bachheimer, Berge, Zeyenk, Van Tendeloo, Van Landuyt & Amelinckx, 1984; Yamamoto, Tsuda & Yagi, 1985, 1988) and very recently for alloys (Fujino, Sato, Hirabayashi, Aoyagi & Koyama, 1987). Yamamoto *et al.* (1988) studied the structures of DC's in the IC phase of the $3-q$ state of quartz and dynamic processes of the 'dislocations' in the triangular domain lattice, such as formation of a pair of 'dislocations', motions of the 'dislocations', their interactions with other 'dislocations' and their annihilations.

However, few electron microscope observations of DC's in ferroelectric substances, which show a variety of IC phases (see Ishibashi, 1986) have been reported. A recent work by Bestgen (1986) on Rb_2ZnCl_4 is one example. Bestgen, however, did not report details of the structures of the DC's and 'dislocations' in Rb_2ZnCl_4. We have carried out detailed studies on Rb_2ZnCl_4 and preliminary results (Tsuda, Yamamoto, Yagi & Hamano, 1986) and details of the dynamics of the DC's and 'dislocations' during the C–IC phase transition (Tsuda, Yamamoto & Yagi, 1988) have been reported.

It is important to know the crystallographic structures of the DC's and 'dislocations' in the IC phase. However, in the IC phase they are narrowly spaced (Tsuda *et al.*, 1988) and electron microscope studies are difficult. One posssible approach is to analyze domain structures in the C phase which are considered to be quenched states of the DC's and 'dislocations' in the IC phase. In the present paper, the domain structures in the C phase are studied through image contrast of the domains and the DC's and their dependence on various reflections excited. The results are consistent with a group-theoretical consideration of the phase transitions and the structure of the C phase.

2. Experimental

Experimental details are given in the paper of Tsuda *et al.* (1988). Here, only the important points are described. Single crystals grown from the melt were used. Thin crystal plates with the (010) surface were cleaved and thinned by a mixture of water and ethyl alchohol. As mentioned previously (Tsuda *et al.*, 1986, 1988) (100) thin plates give weak superlattice reflections in the IC and C phases and they are not useful for the present study.

The thin sample crystals were glued with a silver paste to electron microscope copper grids with a large hole in their centers. A side-entry single-tilt specimen cooling holder is used, which is cooled by liquid N_2 and the temperature is controlled by a small heater in the range between 133 and 343 K with an accuracy of ±5–10 K. In the present paper all of the images, except for diffraction pattern shown in Fig. 1, were taken at 133 K (the C phase). A JEM 200CX electron microscope with accelerating voltage of 200 kV was used. To reduce damage due to the imaging electron beam, its intensity was reduced to 1 mA cm^{-2} during observations.

* Present address: Faculty of Engineering, Technological University of Nagaoka, 1603-1 Kamitomiokamachi, Nagaoka 940-21, Japan.

0108-7673/88/060864-07$03.00

3. Results

3.1. *Electron diffraction pattern*

Fig. 1 reproduces a transmission electron diffraction pattern from the IC phase of Rb_2ZnCl_4. The electron beam is nearly parallel to the [010] direction. Strong spots are fundamental reflections such as 002 and 200 and their extinction agrees with what is expected from the space group of the normal phase (*Pmcn*). In this paper, all of the reflections are indexed using the unit cell of the normal phase except for the discussion in § 4.2. Weak reflections are characteristic of the IC phase. Their positions are close to $h,0,(2n+1)\pm\frac{1}{3}$. The modulation is in the [001] direction and the modulation vector **q** in the IC phase is $(\frac{1}{3}-\delta)c_0^*$ as shown in Fig. 1. The weaker spots are due to second-order reflections and the distance between the two spots is $3\delta c_0^*$. In the C phase, which is ferroelectric with the spontaneous polarization parallel to the [100] direction, $\delta = 0$ and the lattice parameter in the [001] direction is three times that in the normal phase. In some cases diffraction patterns from parts of the specimens of the C phase show reflections at irrational positions, as shown in Fig. 1, which means that in those regions DC's in the IC phase are quenched in the C phase. Most of the micrographs shown in this paper are dark-field images taken with the objective aperture at the positions of one of the superlattice reflections, such as $\pm2,0,\pm\frac{2}{3}$ or $\pm2,0,\pm\frac{4}{3}$.

3.2. *Images of DC's and domains*

Fig. 2 shows a dark-field electron micrograph of an Rb_2ZnCl_4 thin crystal due to the $20\frac{4}{3}$ reflection (**g** in the micrograph) taken at 133 K (the C phase). The [100] and [001] directions in the field of view are illustrated in the image and are the same as in Fig. 1. All of the micrographs in the present paper are illustrated in the same orientation and the indices of the imaging reflections are described using these axes.

Dark lines nearly parallel to the [100] direction are DC's in the C phase, which are equivalent to antiparallel domain boundaries, as will be shown in later sections. A notable fact is that six DC's join together to form a 'dislocation' in the one-dimensional DC lattice at positions indicated by arrows. The observation agrees with the theoretical prediction of DC's by the Landau theory [see, for example, the recent review by Ishibashi (1986)]. These 'dislocations' play an important role during the C–IC phase transiton (Tsuda *et al.*, 1988). As seen in Fig. 1 the DC's have a tendency to form pairs, especially at crystal edges (Tsuda *et al.*, 1988). This is due to a tendency of one of the two possible antiparallel ferroelectric domains to expand (see Fig. 3), caused by a local electric field.

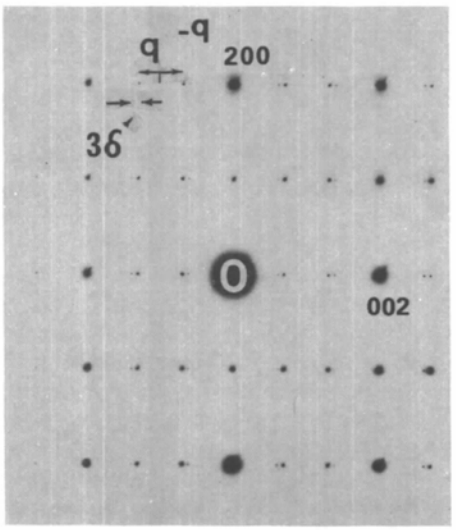

Fig. 1. Electron diffraction pattern from the IC phase of an Rb_2ZnCl_4 thin crystal. The electron beam is parallel to the [010] direction. Spots due to incommensurate modulation with a vector **q** are seen.

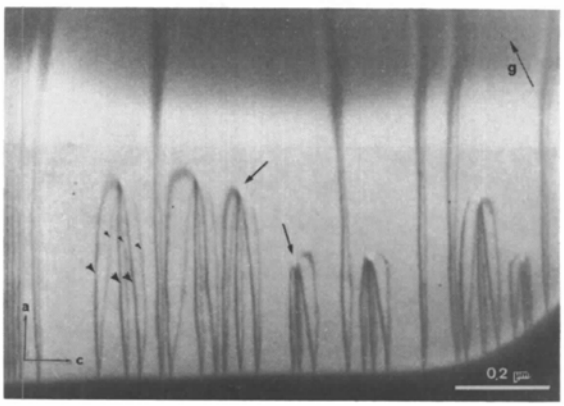

Fig. 2. A $20\frac{3}{4}$ dark-field image of the C phase of an Rb_2ZnCl_4 thin crystal. Dark lines are DC's and 'dislocations' of DC's are seen. Note the alternation of darker image contrast of the DC's.

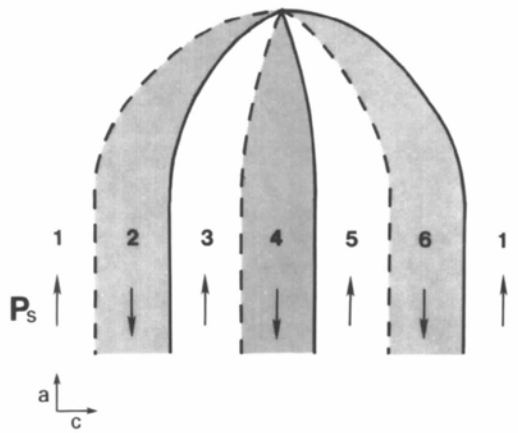

Fig. 3. A schematic illustration of a 'dislocation' of DC's in Rb_2ZnCl_4.

However, the pair was not found to annihilate or to become a single line.

Fig. 3 schematically illustrates the DC configuration at the 'dislocation' and the characteristics of the image contrast of the DC's and the domains between them. If we assume that the spontaneous polarization P_s in a domain denoted by 1 is the [100] direction as shown by an arrow, those in the other domains should be as shown in Fig. 3. A configuration with reversed polarization is also possible.

We look at image contrast between the neighboring antiparallel domains and image contrast of the DC's. In Fig. 2, the former contrast is not seen but the latter is noted; the left-hand members of the pairs are darker than the others, as indicated by large and small arrowheads. This is illustrated in Fig. 3 by broken and full lines.

Fig. 4 shows dark-field images of the same area taken under excitation of different reflections. The image in (*a*) is due to the $20\frac{2}{3}$ superlattice reflection while the images in (*b*) and (*c*) are due to the 200 and $\bar{2}00$ normal reflections, respectively. In (*a*) isolated DC's and closely spaced DC's in an area denoted by *A* are seen. A 'dislocation' is also seen at the position indicated by an arrowhead. In (*b*) and (*c*), however, the isolated DC's and the 'dislocation' are not seen. Only faint contrast of the closely spaced DC's is noted. It was found that the dark-field images due to the 002 reflection (not shown here) do not show isolated DC's. The extinction of the isolated DC's in the fundamental reflection will be discussed in § 4.3. The weak contrast of the closely spaced DC's is due to the higher-order diffraction by the modulated lattice in the closely spaced DC regions.

3.3. *Image contrast experiments for the DC's and the domains*

Image contrast of the domains and the DC's is studied by taking dark-field images due to pairs of superlattice reflections and by comparison of the two images. It is better to take images of the same area for various Bragg settings. However, such a procedure is difficult in the present experiment since the single-

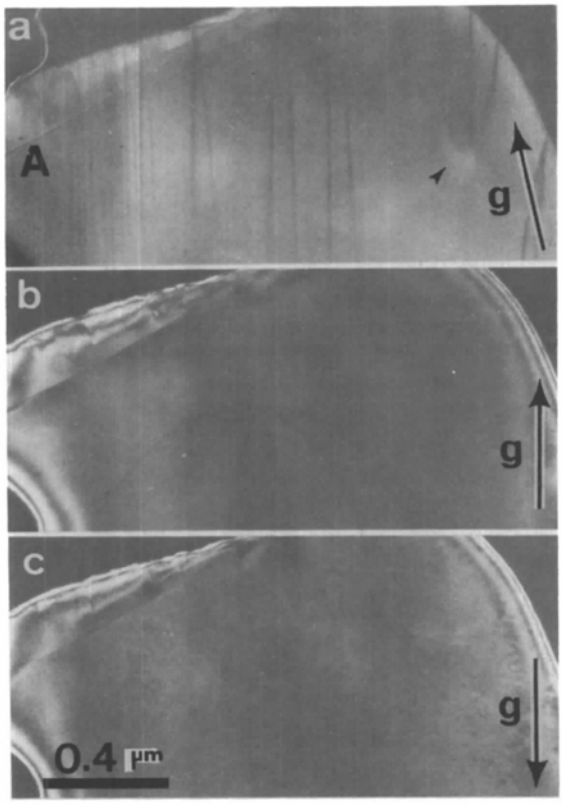

Fig. 4. Dark-field images of the same area due to a superlattice and normal reflections. Note that isolated DC's cannot be seen in the dark-field images due to the normal reflections.

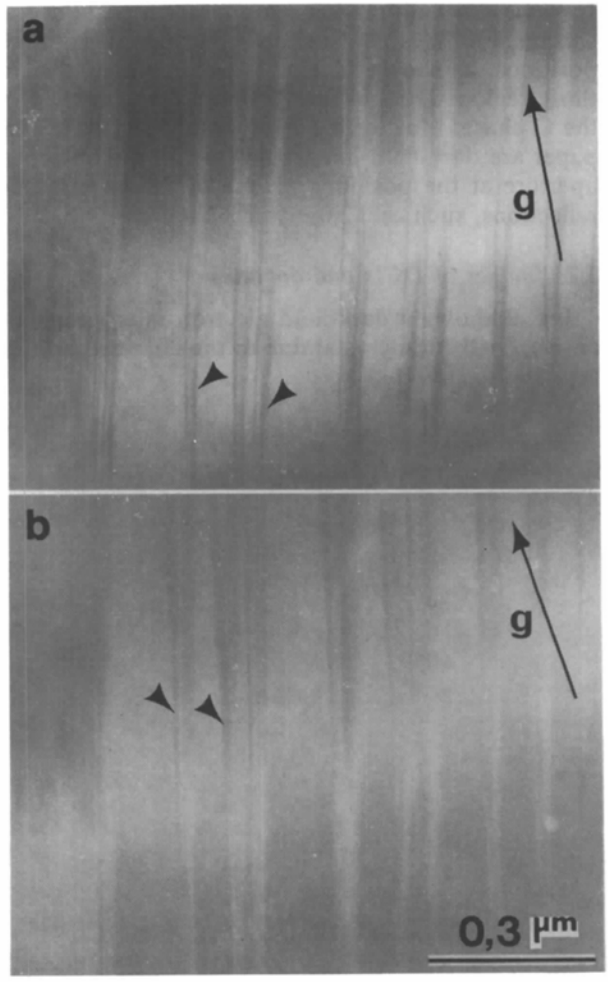

Fig. 5. Dark-field images of the same area due to the $20\bar{\frac{3}{3}}$ and $20\bar{\frac{4}{3}}$ reflections. Note the contrast reversal of pairs of the DC's in the two images.

tilt specimen cooling holder was used and images due to only a pair of the superlattice reflections were taken.

Fig. 5 reproduces dark-field images to make a comparison between the images taken by the $20\bar{\frac{2}{3}}$ and $20\bar{\frac{4}{3}}$ reflections. Since the structure factors of the superlattice reflections are small then their Bragg widths are small, and hence it is difficult to excite these reflections in the whole field of view, especially when the specimen is slightly bent. Therefore, the images are clearly seen only in a restricted zone in the micrographs. This pair of the micrographs represents the case where the modulation vector **q** is reversed as seen in Fig. 1 but the component of the reflection vector parallel to the P_s direction (the P_s component of the reflection vector) is the same for the two images.

In the micrographs DC's form pairs and in Fig. 5(*a*) the right-hand DC's of the pairs are seen to be darker, while in Fig. 5(*b*) the left-hand DC's are darker, as indicated by arrowheads. The domain contrast, which is nearly absent, does not change from (*a*) to (*b*).

Fig. 6 reproduces dark-field images to make a comparison between the images taken by the $20\frac{2}{3}$ and $\bar{2}0\frac{2}{3}$ reflections. In this case the **q** vector is not changed but the P_s component of the reflection vector is reversed. It is noted that neighboring domains have weak contrast in the two micrographs and contrast reverses from (*a*) to (*b*) as indicated by *B* (bright) and *D* (dark). It is also noted that the left-hand DC's of the DC pairs are darker in (*a*) but the right-hand ones are darker in (*b*), as indicated by arrowheads.

Fig. 7 reproduces dark-field images to make a comparison between the images taken by the $\bar{2}0\bar{\frac{2}{3}}$ and the $20\frac{2}{3}$ reflections. In this case the reflection vector is reversed so that the **q** vector and the P_s component of the reflection vector are reversed at the same time. The domain contrast reverses but the DC contrast does not, as indicated by *D*, *B* and arrowheads.

The above three cases indicate that the domain contrast reverses when the P_s component of the reflecting vector is reversed. The domain contrast does not depend on the sign of the **q** vector. In general the contrast is very weak and by a slight deviation from the exact Bragg setting the contrast disappears but contrast reversal does not take place. On the other hand, the reversal of the contrast of the DC pair does not show such a systematic dependence on the reflection vectors.

4. Discussion

4.1. *Group-theoretical consideration of the domain configuration in the C phase*

We follow a method developed by Van Tendeloo & Amelinckx (1974). They showed that a space group *H* of a high-temperature high-symmetry phase can be decomposed using a space group *G* of a low-temperature low-symmetry phase in the

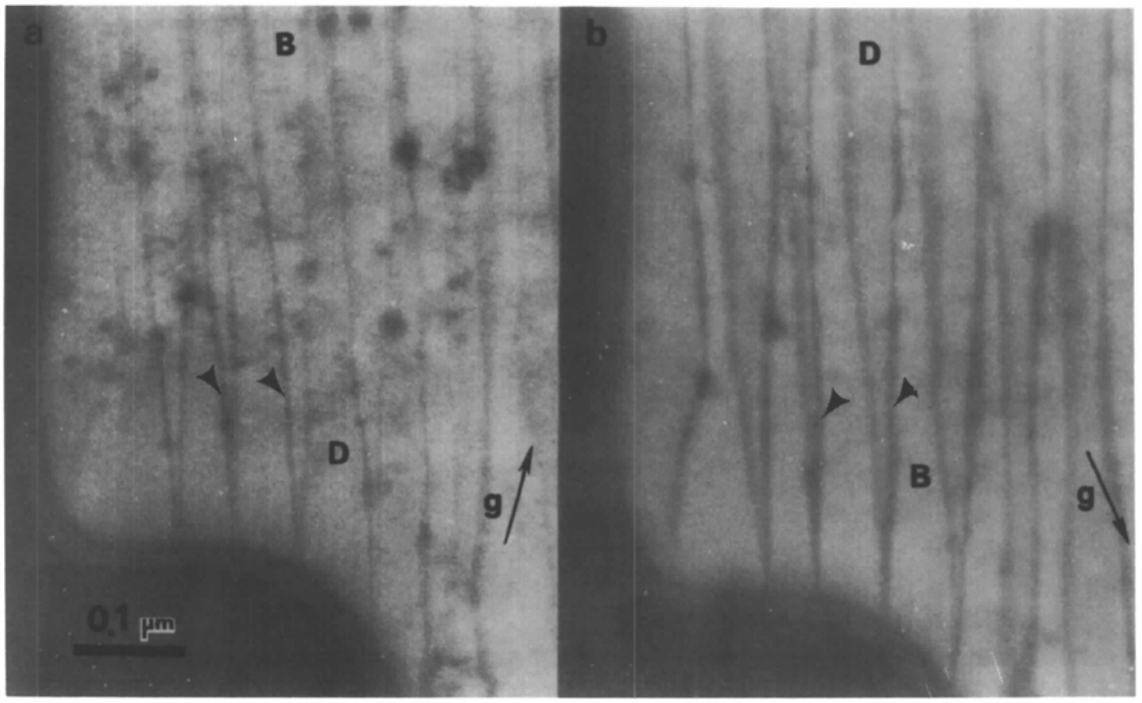

Fig. 6. Dark-field images of the same area due to the $20\frac{2}{3}$ and $20\bar{\frac{2}{3}}$ reflections. Note contrast reversals of domains and pairs of DC's.

following way:

$$H = h_1 G + h_2 G + \ldots + h_p G, \qquad (1)$$

where $h_1 = E$ (identity operation) and the other h_i are elements which belong to H but not to G; p is the ratio $(=n/m)$ of element numbers of H (n) and G (m). P is the number of domains (orientational and translational variants) expected in the low-temperature phase. In the present case H is for the normal phase and is $Pmcn$ $(n=24)$ and G is for the C phase and is $P2_1cn$ $(m=4)$; $p=6$. h_i is expressed as follows:

$$h_1: \; x \; y \; z \; (=E)$$
$$h_2: -x \; -y \; -z \; \text{(inversion)}$$
$$h_3: x \; y \; z+\tfrac{1}{3} \; \text{(translation)}$$
$$h_4: -x \; -y \; -z+\tfrac{1}{3}$$
$$h_5: x \; y \; z+\tfrac{2}{3}$$
$$h_6: -x \; -y \; -z+\tfrac{2}{3}.$$

Here, translations are expressed using the unit cell of the C phase $(c=3c_0)$. It is convenient to write all domains in a right-handed system and in this case h_2, h_4 and h_6 can be expressed as

$$h_2': \; -x \; y+\tfrac{1}{2} \; -z+\tfrac{1}{6}$$
$$h_4': \; -x \; y+\tfrac{1}{2} \; -z+\tfrac{3}{6}$$
$$h_6': \; -x \; y+\tfrac{1}{2} \; -z+\tfrac{5}{6}.$$

It is clear that h_i with i odd gives an out-of-phase domain and h_i with i even gives an antiparallel domain. In § 3 it was shown that: (1) two kinds of domain showing different contrast alternate with each other forming a one-dimensional domain lattice; (2) there are two kinds of DC's showing different contrast, which is closely related to the above alternation; (3) six, and only six, DC's can annihilate to form a pair of 'dislocations'; and (4) there is a tendency of the DC's to form pairs, but they never annihilate (see Fig. 3) nor combine into simple planar defects except at crystal edges. The observation (1) suggests a configuration of alternation of antiparallel ferroelectric domains in the C phase. The fact (2) means that there are two types of DC's, which appear in alternation. The facts (3) and (4) mean that domains with the same phase appear only once in every six domains. The group-theoretical analysis and the observations mentioned above lead to the lattice relations between the successive domains shown in Fig. 8. Thus, in the 'dislocation' structure shown in Fig. 3, six domains should be those shown in Fig. 8, and this configuration is considered to be the frozen structure of the DC's and the 'dislocations' in the IC phase. Other configurations are impossible except for a configuration with reversed order of domains. Domains 3 and 5 are out-of-phase domains with respect to domain 1 and are connected to the domain 1 by h_3 and h_5, and domains 2, 4 and 6 are antiparallel domains with respect to domain 1 and are connected to domain 1 by h_2', h_4' and h_6'. The fact (4) means that simple

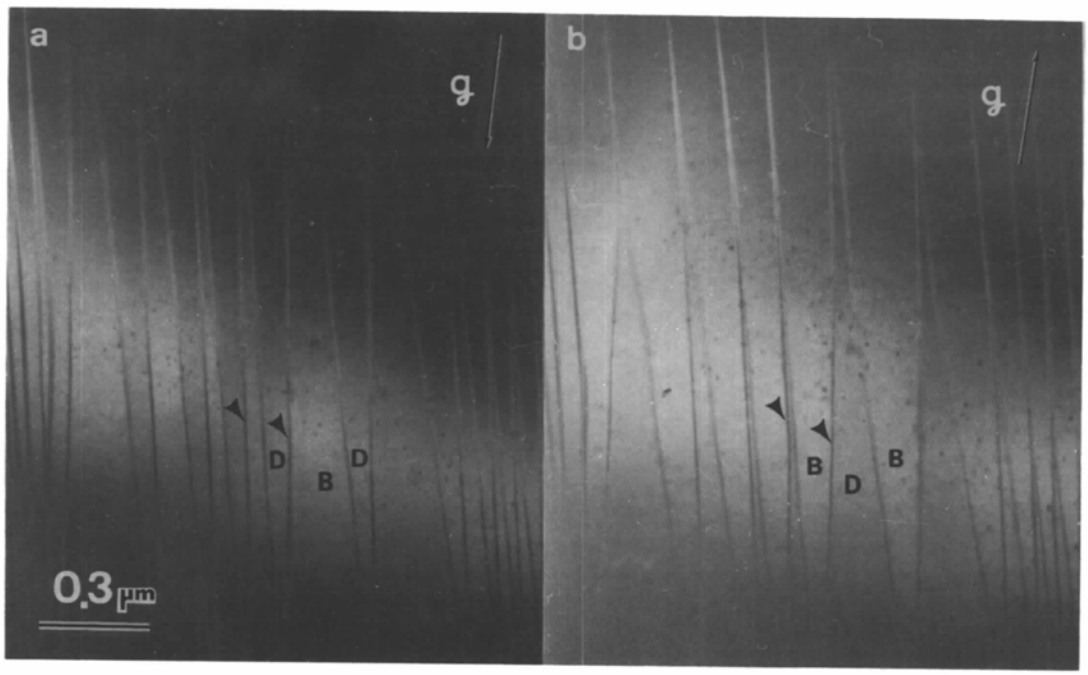

Fig. 7. Dark-field images of the same area due to the $20\frac{2}{3}$ and $\bar{2}0\frac{2}{3}$ reflections. Note the contrast reversal of domains but no contrast reversal of pairs of DC's.

out-of-phase boundaries with a relative displacement $c/3$ ($=c_0$) formed by h_3 are energetically unstable and pairs of DC's are stable.

4.2. *Domain contrast*

Since in the present case domain 1 is connected to the neighboring domains 2 and 6 by the operations h_2' and h_6', the structure factors F_2 and F_6 for the domains 2 and 6 for the reflection $\bar{h}k\bar{l}'$, which is expected to be excited in them following the excitation of the hkl' reflection in domain 1, are given by $F(\bar{h}k\bar{l}')\exp[-2\pi i(k/2+l'/6)]$ and $F(\bar{h}k\bar{l}')\times\exp[-2\pi i(k/2+5l'/6)]$, respectively. Here l' is used instead of l in order to indicate that the superlattice ($c=3c_0$) is used for the third index. For $k=0$ as in the present experiments $F_1^*F_1$ is equal to $F_2^*F_2$ and $F_6^*F_6$ by Friedel's law and domain contrast is not expected. Therefore, the observed weak contrast must be due to the failure of Friedel's law as in the case of $BaTiO_3$ (Tanaka & Honjo, 1964) since other possible reasons for the contrast, such as difference in the excitation error between the neighboring domains, do not exist in the present case.

The present experiment, however, cannot determine the directions of P_s in the observed areas. It should be determined by experiments which intentionally apply an electric field to the specimens.

4.3. *Image contrast of DC's*

From the above considerations it is clear that image contrast of the DC's seen only in the dark-field images of the superlattice reflections is nothing but the α fringe contrast. The fact that the contrast is absent in the dark-field images due to the fundamental reflections indicates that a lattice translation in addition to the expected one from the symmetry consideration, which actually exists in the case of the out-of-phase boundaries in $Gd_2(MoO_4)_3$ (Yamamoto, Yagi & Honjo, 1977), does not exist in the present case. The observed difference in the image contrast of the neighboring DC's, therefore, should be due to a difference in the phase factors of the structure factors of the neighboring domains such as between domains 1 and 6 and domains 1 and 2. The difference in the phase factors can be written as

$$\alpha=\alpha(g)-[\alpha(R^{-1}g)-2\pi gt] \qquad (2)$$

where R is a rotational operation and t is a translational operation, both of which connect the lattices of the neighboring domains.

The α fringe intensity $I_{B,D}$ for bright (B) and dark (D) field images can be expressed in the two-beam case (Amelinckx, 1970) as

$$I_{B,D}=I_{B,D}^{(1)}+I_{B,D}^{(2)}+I_{B,D}^{(3)} \qquad (3)$$

with

$$I_{B,D}^{(1)}=(\tfrac{1}{2})\cos^2(\alpha/2)(\cosh 2\pi\sigma_i z_0\pm\cos 2\pi\sigma_r z_0)$$

$$I_{B,D}^{(2)}=(\tfrac{1}{2})\sin^2(\alpha/2)(\cosh 4\pi\sigma_i u\pm\cos 4\pi\sigma_r u)$$

$$I_{B,D}^{(3)}=(\tfrac{1}{2})\sin\alpha[\sin(2\pi\sigma_r z_1)\sinh 2\pi\sigma_i z_2 \pm\sin(2\pi\sigma_r z_2)\sinh 2\pi\sigma_i z_1$$

where the signs ($\pm$) correspond to bright- and dark-field images, z_1 and z_2 are film thicknesses above and below the fault plane, $z_0=z_1+z_2$ (total film thickness), $2u=z_1-z_2$ and σ_r and σ_i are reciprocals of the effective extinction and absorption distances for the reflection. The first terms $I_{B,D}^{(1)}$ only depend on z_0 and do not represent fringes. For $\alpha=0$ the first term $I_{B,D}^{(1)}$ gives the intensity of the perfect regions. The second term, $I_{B,D}^{(2)}$, gives the background of the fringes, *i.e.* darkness at the central part of the fringes. The third term $I_{B,D}^{(3)}$ gives fringe contrast and does not contribute to the overall contrast of the α fringes. In the present experimental conditions the DC's are nearly parallel to the electron beam and extinction distances for the superlattice reflections are very long, so that the fringes are not seen clearly and it can be said that the darkness of the DC images is determined mainly by the second term, which is proportional to $\sin^2(\alpha/2)$. From the atomic positions determined by Itoh *et al.* (1986) the phase changes given by (2) are calculated for the DC's between domains 1 and 6 (α_1) and domains 1 and 2 (α_2). Table 1 summarizes the $\sin^2(\alpha/2)$ values for various reflections. The pairs seen in Figs. 5 and 6 are the cases between the $20\frac{2}{3}$ and $20\frac{4}{3}$ reflections and between the $20\frac{2}{3}$ and $\bar{2}0\frac{2}{3}$ reflections respectively, and contrast reversal is expected

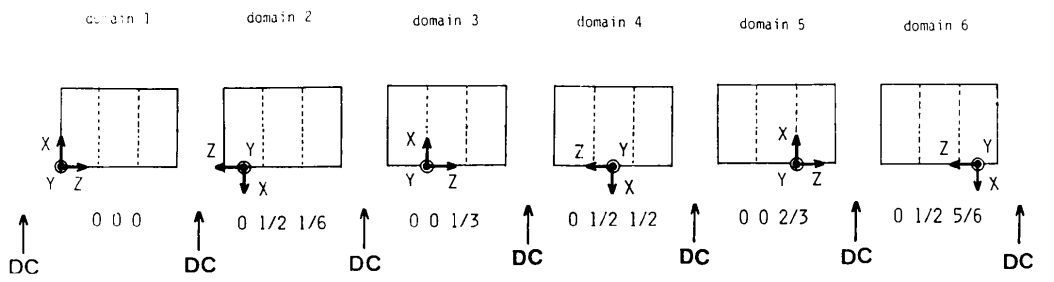

Fig. 8. Schematic illustration of lattice relation between the neighboring domains across the DC's. A right-handed system is assumed.

Table 1. $\sin^2(\alpha/2)$ *values for two types of DC's for various reflections*

h	k	l	$\alpha_1(°)$	$\alpha_2(°)$	$\sin^2(\alpha_1/2)$	$\sin^2(\alpha_2/2)$
2	0	$-\frac{2}{3}$	312·7	72·5	0·161	0·350
2	0	$-\frac{4}{3}$	−96·5	23·4	0·556	0·411
2	0	$\frac{2}{3}$	72·5	312·7	0·350	0·161
−2	0	$\frac{2}{3}$	312·7	72·5	0·161	0·350
−2	0	$-\frac{2}{3}$	72·5	312·7	0·350	0·161

from Table 1, in agreement with the observations. Fig. 7 is the case between the $\bar{2}0\frac{2}{3}$ and $20\frac{2}{3}$, and contrast reversal is not expected, again in agreement with the observations.

From the discussion here it can be said that if the direction of P_s in one domain, say domain 1 in Fig. 3 or 8, is determined by the method mentioned in § 4.2 it will be possible to differentiate a configuration of domains in the order shown in Fig. 8 from that in the reverse order by the contrast analysis of the DC's.

4.4. *Electron diffraction in the IC phase*

From the structural relations between the lattices of the successive domains diffraction spot distributions in the IC phase can be calculated. It was found that asymmetric splitting of the superlattice reflections and their relative intensities were well reproduced.

The authors thank Professor K. Hamano of the Tokyo Institute of Technology for his kind supply of the sample crystals.

References

AMELINCKX, S. (1970). *Modern Diffraction and Imaging Techniques in Material Science*, edited by S. AMELINCKX, R. GEVERS, G. REMAUT & J. VAN LANDUYT, pp. 257-294. Amsterdam: North Holland.

BESTGEN, H. (1986). *Solid State Commun.* **58**, 197-201.

CHEN, C. H., GIBSON, G. M. & FLEMING, R. M. (1982). *Phys. Rev. B*, **26**, 184-205.

DOLINO, G., BACHHEIMER, J. P., BERGE, B., ZEYENK, C. M. E., VAN TENDELOO, G., VAN LANDUYT, J. & AMELINCKX, S. (1984). *J. Phys. (Paris)*, **45**, 901-912.

FUJINO, Y., SATO, H., HIRABAYASHI, M., AOYAGI, E. & KOYAMA, Y. (1987). *Phys. Rev. Lett.* **58**, 1012-1015.

FUNG, K. K., MCKERNAN, S., STEEDS, J. W. & WILSON, J. A. (1981). *J. Phys. C*, **14**, 5417-5432.

ISHIBASHI, Y. (1986). *Incommensurate Phases in Dielectric Materials*, edited by R. BLINC & A. P. LEVANYUK, pp. 49-69. Amsterdam: North Holland.

ITOH, K. *et al.* (1986). Private communication.

MCMILLAN, W. L. (1975). *Phys. Rev. B*, **12**, 1187-1199.

MAHY, J., VAN LANDUYT, J., AMELINCKX, S., UCHIDA, Y., BRONSEMA, K. D. & VAN SMAALEN, S. (1985). *Phys. Rev. Lett.* **55**, 1188-1191.

TANAKA, M. & HONJO, G. (1964). *J. Phys. Soc. Jpn*, **19**, 954-970.

TSUDA, K., YAMAMOTO, N. & YAGI, K. (1988). *J. Phys. Soc. Jpn*, **57**. In the press.

TSUDA, K., YAMAMOTO, N., YAGI, K. & HAMANO, K. (1986). Proc. 11th Int. Congr. Electron Microscopy (Kyoto), Vol. 2, pp. 1233-1234.

VAN TENDELOO, G. & AMELINCKX, S. (1974). *Acta Cryst.* A**30**, 431-440.

YAMAMOTO, N., TSUDA, K. & YAGI, K. (1985). *Jpn. J. Appl. Phys.* **24**, Suppl. 2, 811-813.

YAMAMOTO, N., TSUDA, K. & YAGI, K. (1988). *J. Phys. Soc. Jpn*, **57**, 1352-1364.

YAMAMOTO, N., YAGI, K. & HONJO, G. (1977). *Phys. Status Solidi A*, **44**, 147-160.

Acta Cryst. (1988). A**44**, 870-878

Electron Diffraction Analysis of Polycrystalline and Amorphous Thin Films

BY D. J. H. COCKAYNE

Electron Microscope Unit, University of Sydney, NSW 2006, *Australia*

AND D. R. MCKENZIE

School of Physics, University of Sydney, NSW 2006, *Australia*

(*Received* 12 *January* 1988; *accepted* 25 *April* 1988)

Abstract

A rapid analytical technique has been developed for obtaining the reduced density function, $G(r)$, from polycrystalline and amorphous thin films, using post-specimen scanning and an energy loss spectrometer on a transmission electron microscope. The technique gives on-line analysis of nearest-neighbour distances to an accuracy of 0·02 Å, together with coordination numbers. It has the advantage over X-ray and neutron techniques that the information can be obtained from small (≤ 1 μm diameter) chosen regions of the specimen. Results from neighbouring selected regions can be compared.

1. Introduction

If one were to look for a common thread in the work, so far, of J. M. Cowley and of A. F. Moodie, whether severally or in tandem, it would be found in the

0108-7673/88/060870-09$03.00